Biosensors and Bioelectronics 155 (2020) 112099

Contents lists available at ScienceDirect

Biosensors and Bioelectronics

journal homepage: http://www.elsevier.com/locate/bios

Restriction of intramolecular motions (RIM) by metal-organic frameworks for electrochemiluminescence enhancement:2D Zr_{12}-adb nanoplate as a novel ECL tag for the construction of biosensing platform

Li-Ying Yao, Fang Yang, Gui-Bing Hu, Yang Yang, Wei Huang, Wen-Bin Liang, Ruo Yuan *, Dong-Rong Xiao **

Chongqing Engineering Laboratory of Nanomaterials & Sensor Technologies, College of Chemistry and Chemical Engineering, Southwest University, Chongqing, 400715, PR China

ARTICLE INFO

Keywords:
RIM
Metal-organic frameworks
Biosensor
Mucin 1

ABSTRACT

Herein, a new phenomenon of enhanced electrochemiluminescence (ECL) emission by restricting intramolecular motion in the 2D ultra-thin Zr_{12}-adb (adb = 9,10-anthracene dibenzoate) metal-organic framework (MOF) nanoplate was discovered for the first time. The coordination immobilization of adb in porous ultra-thin Zr_{12}-adb nanoplate endowed the Zr_{12}-adb excellent ECL performance, including stronger ECL signal and higher ECL efficiency relative to those of H_2adb monomers and H_2adb aggregates. In the 2D Zr_{12}-adb nanoplate, the bridging ligand adb was stretched and fixed between two Zr_{12} clusters, which restricted intramolecular rotations and suppressed unnecessary energy loss caused by self-rotation, thereby remarkably improved the ECL intensity and efficiency. More importantly, the porous ultra-thin structure of Zr_{12}-adb MOF nanoplate not only allowed the coreactants to diffuse into the MOF interior, making both internal and external adb be excited, but also shortened the migration distance of electrons, ions, coreactants and coreactant intermediates, which further improved the ECL efficiency of Zr_{12}-adb and overcame the shortcoming of H_2adb aggregates in which the internal luminophores were not easily excited. Regarding the excellent ECL properties above, Zr_{12}-adb nanoplate was selected as a new ECL emitter incorporated with the bipedal walking molecular machine together to fabricate a biosensor for sensitive detection of mucin 1. The enhanced ECL by restriction of intramolecular motions in MOFs provided a new pathway to improve ECL intensity and efficiency, which lighted up a lamp for the design and manufacture of high-performance ECL materials based on MOFs, thus offering new opportunities to develop ultrasensitive ECL biosensors.

1. Introduction

So far, three major types of electrochemiluminescence (ECL) emitters, namely, organic luminophores, nanomaterials and inorganic luminophores, have been extensively investigated. Recently, owing to their superior optoelectronic properties, high quantum yield, structural tailorability and inexpensive cost, organic luminophores (Ko et al., 2018; Ito et al., 2019) have become a good alternative as ECL emitters. To overcome the poor solubility and radical instability of organic luminophores in the aqueous solution, Bard and co-workers have prepared organic micro/nanocrystals through oil-in-water emulsion (Dick et al., 2014) and reprecipitation (Omer and Bard, 2009; Liu et al., 2017, 2018) method, which realized the production of ECL of organic luminophores in aqueous phase. However, there were still some drawbacks of organic micro/nanocrystals, for example, large particle size and aggregation-caused quenching (ACQ) (Huang et al., 2019) issues, which limited ECL efficiency of organic micro/nanocrystals and their application in biosensing. To resolve the problem caused by ACQ, Tang et al. proposed the concept of aggregation-induced emission (AIE) (Luo et al., 2001; Tang et al., 2001) in 2001, which provided an effective strategy for designing highly efficient solid-state fluorescence materials by restriction of intramolecular motions (RIM). Subsequently, Cola (Carrara et al., 2017) observed that the aggregated Pt (II) complex showed stronger ECL emission than that of the isolated molecules, and coined

* Corresponding author.
** Corresponding author.
E-mail addresses: yuanruo@swu.edu.cn (R. Yuan), xiaodr98@swu.edu.cn (D.-R. Xiao).

https://doi.org/10.1016/j.bios.2020.112099
Received 11 December 2019; Received in revised form 2 February 2020; Accepted 12 February 2020
Available online 13 February 2020

this unique phenomenon as "aggregation-induced electrochemiluminescence" (AI-ECL). However, noble metal compounds held the drawbacks of potential biotoxicity, high cost, and poor biocompatibility. Then, Lu's group (Han et al., 2019) and our group (Liu et al., 2019) studied ECL performance of the AIE luminogens and found that the aggregated state had stronger ECL signal than that of the isolated one. These studies indicated that ECL could be obviously enhanced by limiting intramolecular motions. Inspired by above researches, we speculated that restriction of intramolecular motions by metal-organic frameworks (MOFs) could also achieve ECL enhancement. Interestingly, our experimental results demonstrated the validity of our speculation. Therefore, here, we proposed a new and efficient strategy for ECL enhancement, namely RIM by MOFs for ECL enhancement.

As a prevailing class of solid porous materials, MOFs possess well-ordered porosity, ultrahigh surface area and structural tunability (Jiang et al., 2018; Chen et al., 2011; Xiao et al., 2012; He et al., 2011, 2012; Li et al., 2017), which make them promising carrier materials to enhance the loading number of luminophores for enhancing ECL intensity and efficiency. Recently, MOFs have been used to stably immobilize ECL luminophores to increase the ECL response and improve the sensitivity of ECL sensors (Hu et al., 2018; Xiong et al., 2017; Jiang et al., 2017b). However, almost all reported MOFs-based ECL materials were synthesized from the immobilization of $Ru(bpy)_3^{2+}$ and its derivatives into MOFs by doping or postsynthetic methods. As we all know, Ru-complexes are costly and have large steric hindrance, which limits the immobilization capacity to some extent and increases the difficulty of loading. Hence it is desirable and significant to develop Ru-complex-free MOFs-based ECL materials with superior ECL property. Moreover, it has been reported that the inhibition of the intramolecular rotation in the 9,10-diphenylanthracene derivatives could greatly improve the fluorescence efficiency (Hong et al., 2011; Iida and Yamaguchi, 2009). Inspired by this, we attempted to immobilize the adb (adb = 9,10-anthracene dibenzoate) in MOFs to limit intramolecular rotation and expected to achieve ECL enhancement. Following this strategy, a novel ECL emitter, namely Zr_{12}-adb nanoplate, was synthesized by the coordination of bridging ligand adb and Zr_{12} clusters, which showed a superb and stable anodic ECL emission with a high ECL efficiency. The possible reasons for the enhanced ECL could be analyzed from the structure of Zr_{12}-adb nanoplate as follows. (1) The bridging ligands adb were immobilized in the Zr_{12}-adb MOF, which inhibited non-radiative decay involving intramolecular rotation, vibration, and torsion, thereby greatly enhancing the ECL intensity and efficiency. Meanwhile, the immobilization content of adb luminophores was greatly increased since adb was directly used as ligands. (2) The ultrathin thickness of

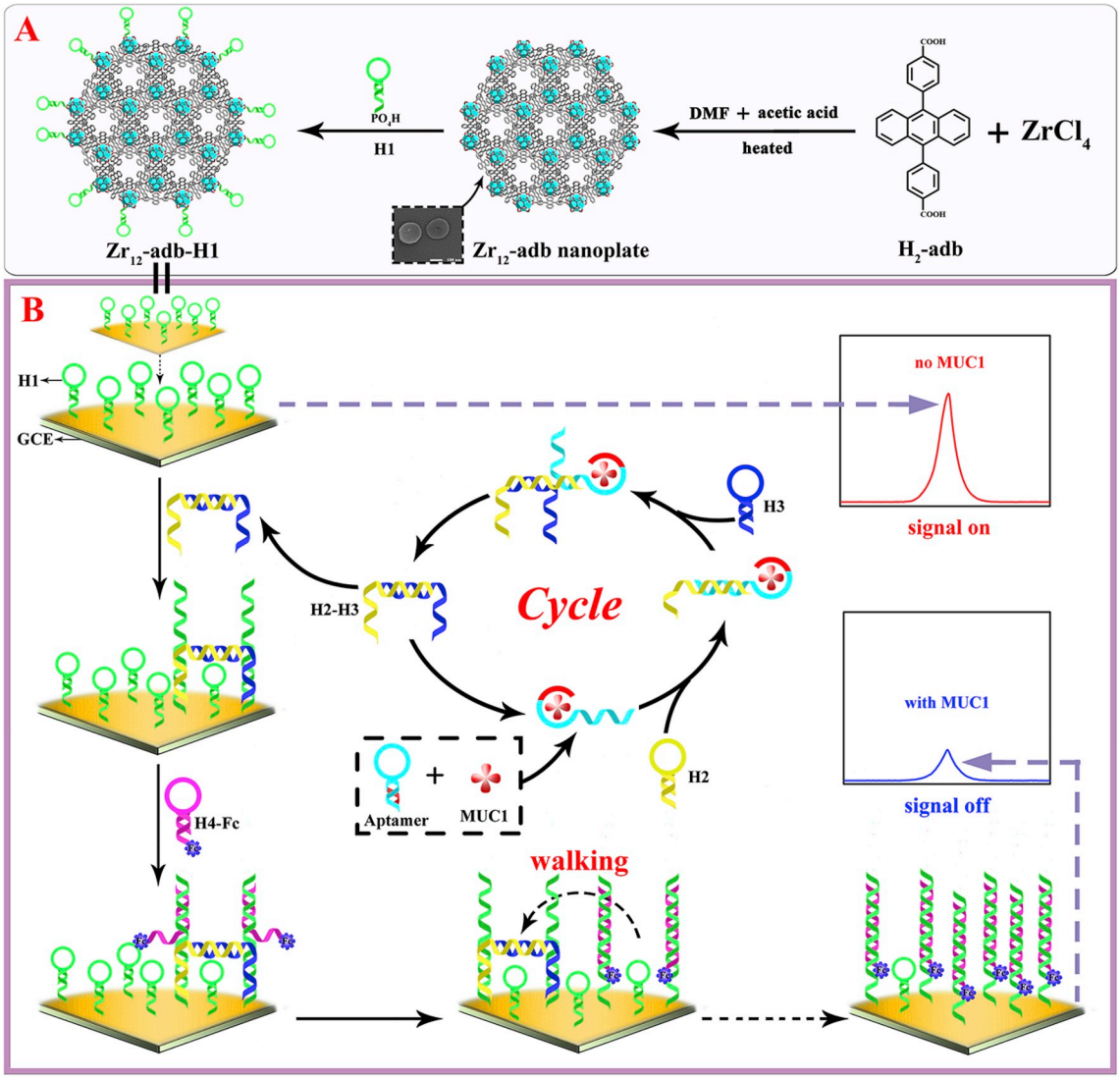

Scheme 1. (A) The prepared process of Zr_{12}-adb-H1. (B) The fabrication procedure of the developed biosensor.

Zr_{12}-adb MOF highly shortened the diffusion distance of the ions, electrons, coreactants and coreactant intermediates. Moreover, the porous matrix enabled the internal and external adb to be electrically activated and interacted with coreactant (tripropylamine, TPrA), which could effectively improve the utilization ratio of the luminophores. Based on the above advantages, Zr_{12}-adb nanoplates could be used as an ideal sensing platform for biomolecular detection.

Mucin 1 (MUC1) is considered as a biomarker of several cancers because of its overexpression in tumors (Kufe, 2009). The accurate and quantitative detection of MUC1 is of great significance for the early diagnosis of cancers. Here, a novel ECL biosensor was fabricated to determinate MUC1 by using Zr_{12}-adb nanoplate as an excellent ECL emitter combined with the amplification strategy of the bipedal walking molecular machine (BWMM) (Tomov et al., 2017). Initially, as shown in Scheme 1A, the Zr_{12}-adb nanoplate was prepared by solvothermal method with $ZrCl_4$ and H_2adb. Subsequently, phosphate-terminal hairpin DNA 1 (H1) was modified on the surface of Zr_{12}-adb nanoplate by strong coordination bonds between phosphate and zirconium (Liu et al., 2018; Wang et al., 2017). The synthesized Zr_{12}-adb-H1 was then dripped onto the electrode surface to produce a strong initial ECL signal (signal-on) with the TPrA coreactant. The specific construction process of the biosensor was displayed in Scheme 1B, with the help of hairpin DNA 2 (H2) and hairpin DNA 3 (H3), the target MUC1 was converted into numerous H2–H3 BWMM through the specific recognition between MUC1 and its aptamer. Then, the "feet" parts of H2–H3 could open and hybridize with the locked stem of H1 to expose the previously locked toehold portion of H1. Meanwhile, the ferrocene-labeled hairpin DNA 4 (H4-Fc) was introduced and hybridized with the H1 through toehold-mediated strand displacement processes, and the H2–H3 was released and repeated the above procedures. As a result, mickle H1–H4-Fc were formed in the sensing interface to quench the ECL and gain "signal-off" state. As expected, the proposed biosensor accomplished facile and sensitive detection of MUC1. It is believed that the discovery of RIM by MOFs for ECL enhancement provides a new and effective strategy for the design and synthesis of high-performance ECL emitters, thus revealing a new path to devise highly sensitive ECL biosensors.

2. Experimental

2.1. Materials and instruments

The materials and instruments involved in this work were supplemented in the supporting information.

2.2. The preparation of Zr_{12}-adb-H1 conjugates

Zr_{12}-adb nanoplate was prepared according to previous report (Dai et al., 2017), except that H_2adb was used instead of 2′-nitro-[1,1′:4′,1″-terphenyl]-4,4″-dicarboxylic acid (H_2TPDC-NO_2) during the synthesis. Initially, 7.5 mg H_2adb, 4.2 mg $ZrCl_4$, 10 mL DMF and 0.75 mL glacial acetic acid were mixed in a vial. Then, the mixture was sonicated for 10 min to disperse all solids evenly and kept at 80 °C for 48 h. The resultant yellow suspension was collected by centrifugation and washed several times with DMF and THF, respectively. Finally, the yellow product was dried under vacuum at 50 °C to obtain yellow powder for subsequent use.

Before using, the phosphate-terminal hairpin 1 (H1) was annealed at 95 °C in Tris-HCl buffer for 5 min and then cooled down to ambient temperature slowly. Then, 300 μL 100 μM annealed H1 and 2 mg freshly prepared Zr_{12}-adb nanoplates were dispersed in 1 mL DMF. The mixture was incubated overnight on a shaker at room temperature. In order to reduce electrostatic repulsion between neighboring H1 and get high densities of H1 in the surface of Zr_{12}-adb nanoplate, sodium chloride was slowly added into the mixture to a final concentration of 0.5 M. The resultant was washed with ultrapure water and centrifuged at 5000 rpm for 10 min to remove free H1. Eventually, the obtained Zr_{12}-adb-H1 conjugates were dispersed in 1 mL ultrapure water for subsequent application.

2.3. The fabrication of ECL sensing interface

Prior to modification, the glass carbon electrode (GCE, Φ = 4 mm) was pretreated with the previous method (Zeng et al., 2018; Zhuo et al., 2014). Briefly, the bare GCE was polished with 0.3 and 0.05 μm α-alumina powder followed by sonication in ethanol and ultrapure water respectively to get a clear mirror-like surface. After that, 5 μL Zr_{12}-adb-H1 conjugates were dropped on the clear surface of GCE and dried in ambient temperature to gain a uniform layer.

2.4. Measurement procedure

Firstly, MUC1 aptamer, hairpin 2 (H2), hairpin 3 (H3), Fc-labeled hairpin 4 (H4-Fc) were annealed at 95 °C for 5 min and then cooled down slowly to ambient temperature, respectively. After that, 20 μL of the mixture solution containing 2 μM aptamer, 2 μM H2, 2 μM H3 and various concentrations of MUC1 was incubated for 30 min on a shaker at room temperature to form abundant H2–H3 duplexes. Then the mixture was dropped on the modified electrode (Zr_{12}-adb-H1/GCE) and maintained 2 h at room temperature. After being rinsed with PBS solution (0.1 M, pH = 7.4), the ECL response of biosensor was measured in 2 mL PBS solution containing 2 mM TPrA with the scanning potential from 0 V to 1 V, and the scanning rate was 0.3 V/s.

3. Results and discussion

3.1. SEM and XRD characterization of Zr_{12}-adb and Zr_{12}-adb-H1

In order to characterize the prepared Zr_{12}-adb and Zr_{12}-adb-H1, we used scanning electron microscopy (SEM) to observe their morphologies and sizes. As shown in Fig. 1A and B, Zr_{12}-adb exhibited a round nanoplate shape with a diameter of 100–200 nm and a thickness of about 20 nm. Additionally, as exhibited in Fig. 1C, powder X-ray diffraction (PXRD) was used to characterize the structure of Zr_{12}-adb, which showed that Zr_{12}-adb adopted Zr_{12}-TPDC (TPDC = terphenyl dicarboxylate) topology with the PXRD pattern matching that of Zr_{12}-TPDC (Dai et al., 2017). All of the above characterizations demonstrated the successful preparation of Zr_{12}-adb nanoplate.

To prove the successful synthesis of Zr_{12}-adb-H1, the zeta potential of Zr_{12}-adb and Zr_{12}-adb-H1were measured respectively by a dynamic laser light scattering. As shown in Fig. S1A, the zeta potential of Zr_{12}-adb was positive with an average of 20.9 mV. However, due to H1 was negative, the zeta potential of Zr_{12}-adb-H1 was negative with an average of −12.9 mV, which demonstrated that the H1 was coordinated to the vacant locus of Zr_{12} clusters and the Zr_{12}-adb-H1 was prepared successfully. Then, the SEM and EDS mapping were employed to characterize Zr_{12}-adb-H1. As depicted in Fig. S2A, Zr_{12}-adb-H1 exhibited a shape of round nanoplates and EDS mapping revealed that C, O, Zr, and P were uniformly distributed in the synthesized Zr_{12}-adb-H1 nanoplate, and EDS spectrum of the Zr_{12}-adb-H1 showed the peaks of C, O, Zr and P elements (Fig. S2F), which suggested that the Zr_{12}-adb-H1 was prepared successfully.

3.2. Optical characterization of Zr_{12}-adb nanoplates

The optical properties of Zr_{12}-adb nanoplates were explored by ECL spectral analysis and photoluminescence (PL), respectively. As exhibited in Fig. 2A, at a scan potential of 0–1 V, the 3D color map of Zr_{12}-adb was recorded according to the evolution and devolution of its ECL emission. As exhibited in Fig. 2B, the typical heat map image of ECL emission from Zr_{12}-adb was also plotted to observe its maximum emission wavelength intuitively. It could be observed that the maximum emission wavelength

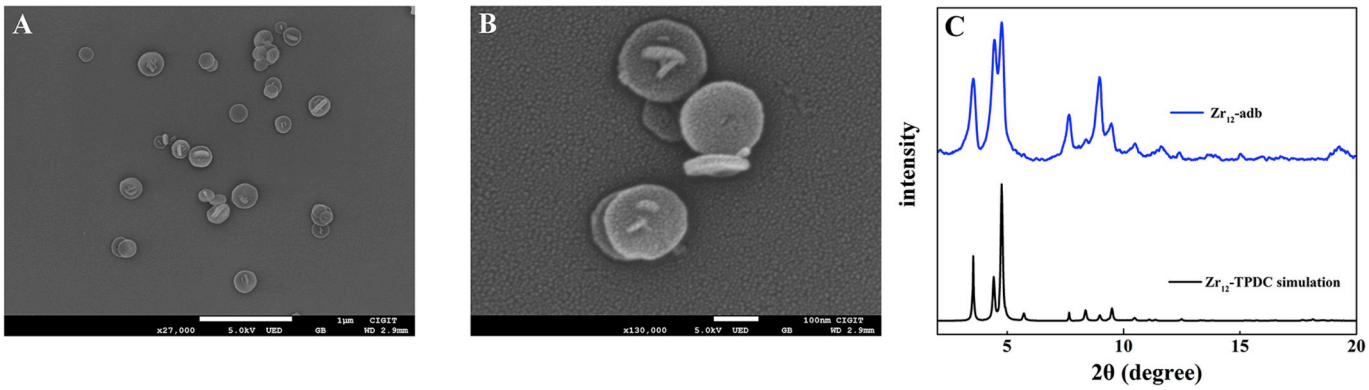

Fig. 1. (A, B) The SEM images of Zr_{12}-adb. (C) The simulated PXRD pattern of Zr_{12}-TPDC and PXRD pattern of Zr_{12}-adb.

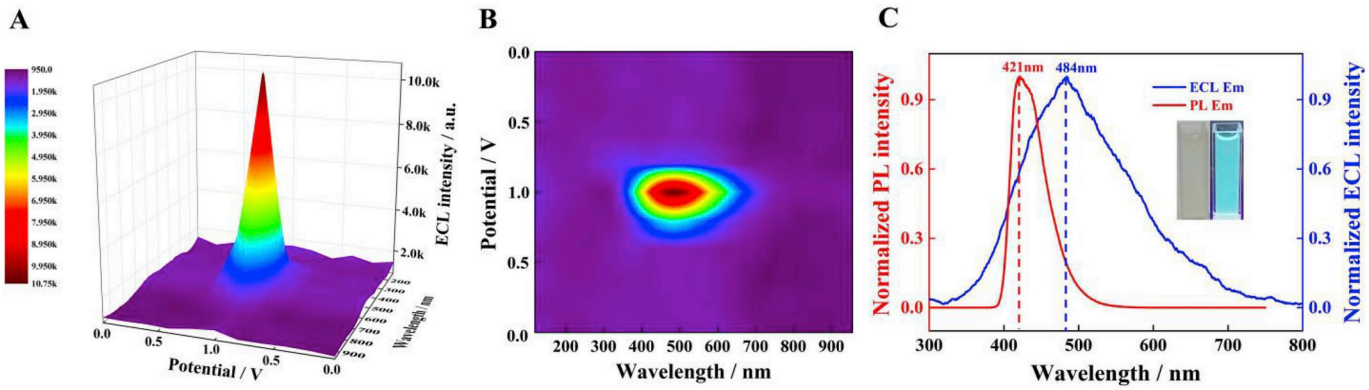

Fig. 2. (A) The 3D color map surface image of ECL-potential-wavelength and (B) the ECL heat map image from Zr_{12}-adb. (C) The normalized ECL emission spectrum (curve blue) and PL emission spectrum at exicitation wavelength of 377 nm. Inset images of C: Zr_{12}-adb under the ambient daylight (left) and the 365 nm UV light (right). (For interpretation of the references to color in this figure legend, the reader is referred to the Web version of this article.)

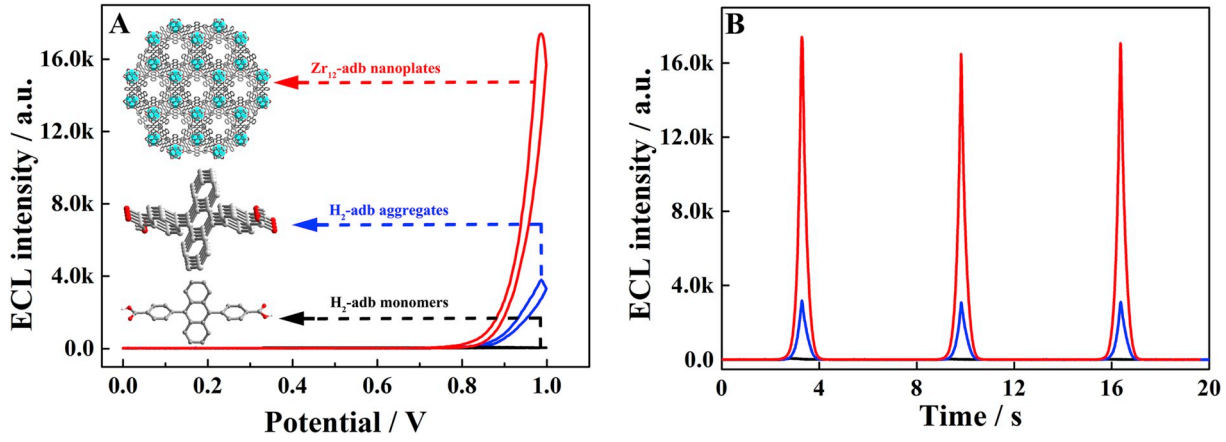

Fig. 3. (A) ECL-potential profiles of different ECL tags (black curve: 0.1 M $(TBA)BF_4$ DMSO solution containing 1 mM H_2adb. blue curve: 0.1 M PBS solution containing 1 mM H_2adb. red curve: 0.1 M PBS solution of Zr_{12}-adb containing 1 mM adb) and its corresponding ECL-time profiles (B). (For interpretation of the references to color in this figure legend, the reader is referred to the Web version of this article.)

was located at 484 nm. Moreover, the PL was investigated and the emission peak was at 421 nm under the excitation wavelength of 377 nm (Fig. 2C), the ECL emission has a distinct red shift of 63 nm compared to PL emission, which may be the instrumental effects and causes of self-absorption (Rashidnadimi et al., 2008; Swanick et al., 2015). In addition, the inset of Fig. 2C exhibited photographs of the Zr_{12}-adb aqueous solution with the radiation of natural light and UV light. It could be observed that the Zr_{12}-adb solution was white under ambient light but was faintly blue under the UV light ($\lambda = 365$ nm).

3.3. Exploration of ECL performance and possible ECL mechanism for Zr_{12}-adb

In addition, the ECL performances of individual H_2adb molecules, H_2adb aggregates and Zr_{12}-adb nanoplates were investigated. As shown in Fig. 3A, with a pulse potential of 0–1 V, almost no anodic ECL response (black curve) was observed for individual H_2adb molecules in 0.1 M (TBA)BF_4 DMSO solution containing 20 mM TPrA as coreactant. When the H_2adb aggregates were dispersed in 0.1 M PBS solution, ECL response showed an obvious improvement compared with that of individual H_2adb molecules. Interestingly, there was a significantly stronger ECL emission when adb was immobilized in the Zr_{12}-adb MOF nanoplate, compared with those of individual H_2adb molecules and H_2adb aggregates. And the identical result was exhibited in ECL-time profile (Fig. 3B). The reasons for ECL enhancement might be ascribed to the following three aspects: primarily, adb was immobilized in the Zr_{12}-adb MOF nanoplate as a bridging ligand, which limited intramolecular motion and increased the immobilization number of adb, thereby suppressing the non-radiative relaxation, reducing unnecessary energy consumption and improving ECL efficiency and intensity. Secondly, due to the concentration enrichment of coreactants (TPrA) in micropores of Zr_{12}-adb nanoplate, the distance between coreactants and adb luminophores was shortened, which allowed the electrochemical activation of the internal and external adb and increased the utilization ratio of adb. Thirdly, ultrathin nature of Zr_{12}-adb nanoplate could also accelerate transfer of electron, ions, coreactants and coreactant intermediates, which led to a further ECL enhancement.

The possible ECL mechanisms of Zr_{12}-adb/TPrA system were described as follows:

$$Zr_{12}\text{-adb} - e^- \rightarrow Zr_{12}\text{-adb}^+ \quad (1)$$

$$TPrA - e^- \rightarrow TPrA^{\bullet +} \quad (2)$$

$$TPrA^{\bullet +} \rightarrow TPrA^{\bullet} + H^+ \quad (3)$$

$$Zr_{12}\text{-adb}^+ + TPrA^{\bullet} \rightarrow Zr_{12}\text{-adb}^* + \text{products} \quad (4)$$

$$Zr_{12}\text{-adb}^* \rightarrow Zr_{12}\text{-adb} + h\nu \quad (5)$$

3.4. ECL efficiency of the Zr_{12}-adb nanoplates

ECL efficiency (the number of photons per electron transferred) was a vital evaluation of ECL property, here we calculated the ECL efficiency of Zr_{12}-adb nanoplate by the following formula (Wang et al., 2016):

$$\varnothing_x = \varnothing_{st}\left(\frac{\int_0^t Idt}{\int_0^t idt}\right)_x \Big/ \left(\frac{\int_0^t Idt}{\int_0^t idt}\right)_{st} \quad (6)$$

$\varnothing_{st}$ was the ECL efficiency of $[Ru(bpy)_3]^{2+}$ (1 mM and 0.1 M (TBA)BF_4/CH_3CN) via annihilation, taken as 5.0%, I was ECL intensity, i stood for current value, and x represented the sample. As shown in Table 1, the ECL efficiency of Zr_{12}-adb nanoplate was ~2.77-fold higher than that of H_2adb aggregates and ~18.59-fold higher than that of H_2adb monomers, which illustrated that Zr_{12}-adb nanoplates held a higher utilization ratio of adb luminophores and demonstrated that RIM by MOFs for ECL enhancement is an efficient strategy to remarkably improve the ECL efficiency.

Table 1
Comparation of ECL efficiency for different materials.

materials	$\varnothing_{ECL}$ (%)	references
Mn@CdInS/TPrA	0.8	Wang et al. (2016)
$Ru(bpy)_3Cl_2$/1 mM (annihilation)	5	
Ru-HPNSs	7.2	Chen et al. (2017)
H_2adb monomers/TPrA	0.98	This work
H_2adb aggregates/TPrA	6.57	
Zr_{12}-adb nanoplates/TPrA	18.22	

3.5. Optimization of reaction conditions

In this work, many experimental parameters played important roles in the performance of biosensors. Therefore, to achieve the optimal performance of the proposed biosensor, incubation time and H4-Fc concentration were optimized. The ECL intensity varied when we adjusted the incubation time (Fig. 4A). It could be seen that the ECL response declined with the extension of incubation time and trended to a plateau at 120 min. Therefore, the incubation time was determined to be 120 min for subsequent experiments. In addition, the concentration of H4-Fc directly affected the degree of annihilation of the ECL signal, which in turn affected the detection range and the detection limit of the proposed biosensor. As shown in Fig. 4B, with the increase of H4-Fc concentration, a gradual decreased ECL response appeared and reached a platform at 1.5 μM, which was selected as the optimal H4-Fc concentration in this work.

3.6. ECL and CV characterizations of the proposed biosensor

To confirm the successful construction of the proposed biosensor, the ECL response was performed to characterize the construction process in 2 mL PBS solution containing 2 mM TPrA. As shown in Fig. 5A, the bare GCE had almost no ECL response (curve a). The ECL signal was enhanced significantly after Zr_{12}-adb-H1 was modified on the surface of GCE (curve b). However, when a mixture of MUC1, MUC1 aptamer, H2, H3 and H4-Fc was incubated on the modified GCE, there was a reduced ECL response obviously (curve c), which could be speculated that quenching probe H4-Fc hybridized with H1 and cause a decreased ECL signal.

In addition, cyclic voltammetric (CV) was also implemented to verify stepwise modification of the biosensor in 5 mM $[Fe(CN)_6]^{3-/4-}$ solution (Fig. 5B). There was a pair of clear redox peaks of $[Fe(CN)_6]^{3-/4-}$ with the bare GCE (curve a). Nevertheless, the CV response was decreased when the Zr_{12}-adb-H1 was modified on the GCE due to the electrostatic hindrance of Zr_{12}-adb-H1 (curve b). Afterward, CV signal was further reduced when a mixture of MUC1, MUC1 aptamer, H2, H3 and H4-Fc was incubated on the modified GCE because of these biomacromolecules with poor conductivity (curve c). The results of the CV measurement and ECL characterization consistently proved the successful fabrication of the proposed biosensor.

3.7. Determination performance of the proposed biosensor

Under optimal conditions, the detection performance of the proposed biosensor was evaluated by incubating a range of concentrations of MUC1 in 2 mL PBS solution containing 2 mM TPrA. As shown in Fig. 6A, the ECL intensity went down with the increment of MUC1 concentrations from 1 fg mL^{-1} to 100 ng mL^{-1}. Moreover, it could be found from Fig. 6B that the amount of change in ECL was positively correlated with the logarithm of MUC1 concentration. The calibration curve equation of the biosensor was $\Delta I = 1027.07 \lg c + 6369.70$ following a linear correlation coefficient of R = 0.9988, and the detection limit was estimated to be 0.25 fg mL^{-1} referring to the 3σ rule (Dixit

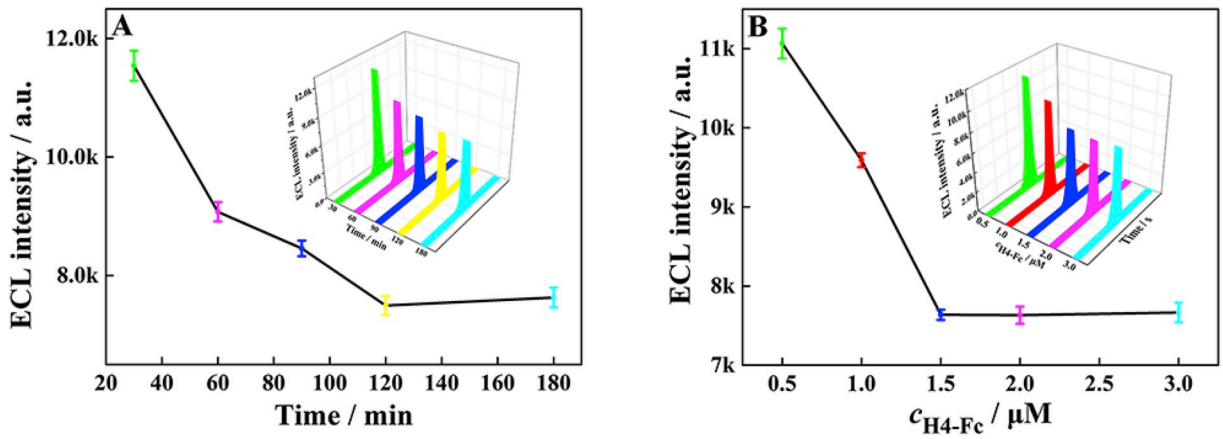

Fig. 4. Experimental optimizations of the developed biosensor for MUC1 detection: (A) the incubation time of bipedal walker and (B) the concentration of H4-Fc.

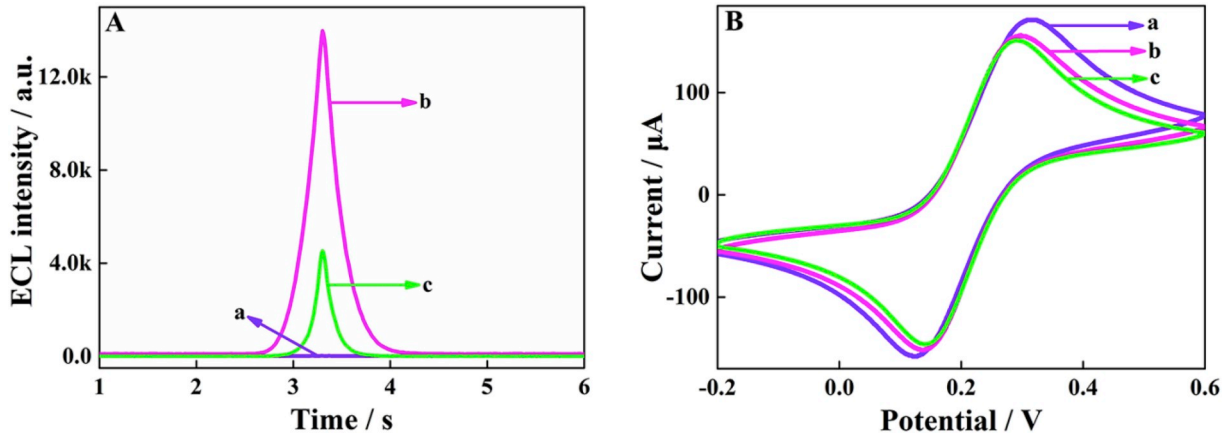

Fig. 5. (A) ECL response of (a) bare GCE, (b) Zr_{12}-adb-H1/GCE, (c) the mixture (1 ng mL^{-1} MUC1, H2, H3, H4-Fc)/Zr_{12}-adb-H1/GCE. (B) CV characterizations of (a) bare GCE, (b) Zr_{12}-adb-H1/GCE, (c) the mixture (1 ng mL^{-1} MUC1, H2, H3, H4-Fc)/Zr_{12}-adb-H1/GCE.

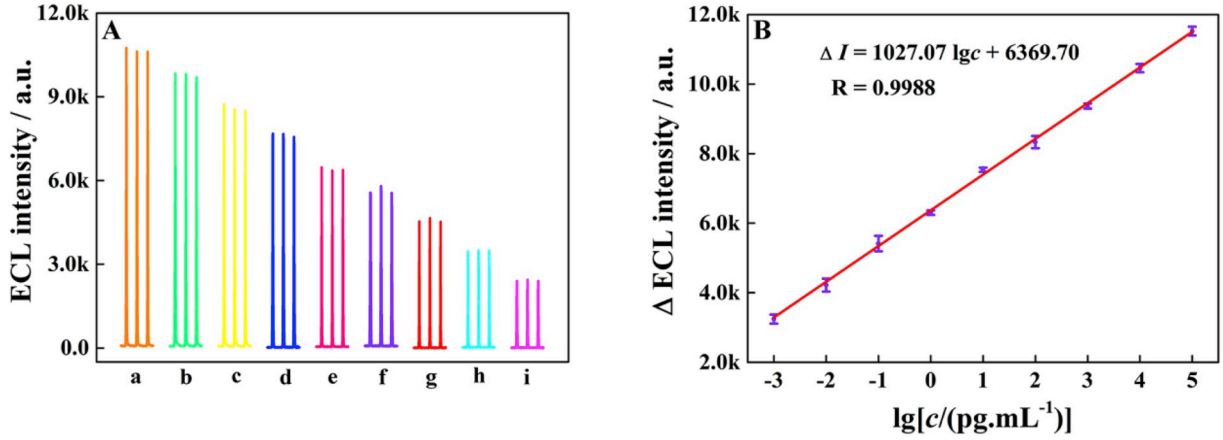

Fig. 6. (A) The ECL response of the proposed biosensor incubated with different concentrations of MUC1: (a) 1 fg mL^{-1}, (b) 10 fg mL^{-1}, (c)100 fg mL^{-1}, (d) 1 pg mL^{-1}, (e) 10 pg mL^{-1}, (f) 100 pg mL^{-1}, (g) 1 ng mL^{-1}, (h) 10 ng mL^{-1}, (i) 100 ng mL^{-1}. (B) The calibration curve for the relationship between the Δ ECL intensity and the logarithm of various MUC1 concentration.

Table 2
Comparison of different methods for detecting MUC1.

detection method	linear range	detection limit	ref
EC	1 nM to 1 μM	0.827 nM (0.25 μg mL^{-1})	Deng et al. (2017)
fluorescence	1 pg mL^{-1} to 20 ng mL^{-1}	0.23 pg mL^{-1}	Yang et al. (2018)
ECL	1 fg mL^{-1} to 1 ng mL^{-1}	0.62 fg mL^{-1}	Jiang et al. (2017a)
ECL	1 fg mL^{-1} to 10 ng mL^{-1}	0.48 fg mL^{-1}	Hu et al. (2019)
ECL	1 fg mL^{-1} to 100 ng mL^{-1}	0.25 fg mL^{-1}	this work

et al., 2010). As displayed in Table 2, our proposed biosensor held a more superior detection sensitivity and a wider detection range compared with the previously reported detection method for MUC1.

3.8. Selectivity, stability and reproducibility of the proposed biosensor

As we all know, the selectivity, stability and reproducibility were important performances of biosensors. Thus, different interfering substances including carcino-embryonic antigen (CEA), β2-microglobulin (β2-MG), α-1-fetoprotein (AFP) were used to evaluate the selectivity of the developed biosensor. As displayed in Fig. 7A, the ECL responses of these interfering substances were almost the same as the blank sample (no target MUC1). Moreover, the mixture of 1 pg mL^{-1} target MUC1 and these interfering substances (10 pg mL^{-1} CEA, 10 pg mL^{-1} β2-MG, 10 pg mL^{-1} AFP) exhibited almost no difference with 1 pg mL^{-1} target MUC1. The experimental results showed that the biosensor owned excellent selectivity for target MUC1.

Furthermore, the stability and reproducibility of the developed biosensor were explored. Firstly, the biosensor was incubated with 100 pg mL^{-1} MUC1 and scanned continuously for 20 times. It could be found that the ECL signals showed a small difference (RSD = 0.98%) in Fig. 7B. Subsequently, the reproducibility was assessed by detecting 5 electrodes at 1 ng mL^{-1} MUC1 and the RSD value was only 0.92% (Fig. 7C). The above results suggested that the developed biosensor had superior stability and reproducibility.

3.9. Determination of MUC1 in human serum

As another considerable performance of biosensor, the practicality was investigated by recovery assay based on standard addition method. Briefly, the human serum was diluted 40 times with PBS (pH = 7.4) and then used for preparation of different concentrations of MUC1. Then, the biosensors incubated with different concentrations of MUC1 were detected by the ECL signals, and the found concentrations were calculated according to the linear equation. As shown in Table 3, the recoveries varied from 97.3% to 100.7%, showing that the developed biosensor held remarkable application potential in clinical diagnosis and treatment.

Table 3
Recovery of MUC1 in human serum.

Samples	Added (pg.mL^{-1})	Found(pg.mL^{-1})	RSD(%)	Recovery(%)
1	0.1	0.0993	0.44	99.3
2	10	9.73	2.94	97.3
3	1000	1006	0.64	100.6
4	10000	10070	3.84	100.7

4. Conclusion

In summary, a new and efficient strategy to enhance ECL, named RIM by MOFs for ECL enhancement, was proposed for the first time. The bridging ligands adb were immobilized in the Zr_{12}-adb MOF nanoplate to hamper the intramolecular motion of adb, thereby suppressing non-radiative energy consumption and improving ECL intensity and efficiency. Furthermore, the porosity and ultra-thin feature of Zr_{12}-adb could accelerate migration of the ions, electrons, coreactants and coreactant intermediates and made the internal and external adb to be electrically activated, which further increased utilization ratio of adb and improved ECL efficiency. In view of the excellent ECL properties, Zr_{12}-adb was employed as a bright ECL tag, combined with BWMM, fabricated an "on-off" biosensor and achieved sensitive determination for MUC1. In short, our work not only opened up a new horizon for exploring novel strategies to enhance ECL, but also expanded the application of MOFs in bioassays and provided an unprecedented idea to devise outstanding ECL emitters.

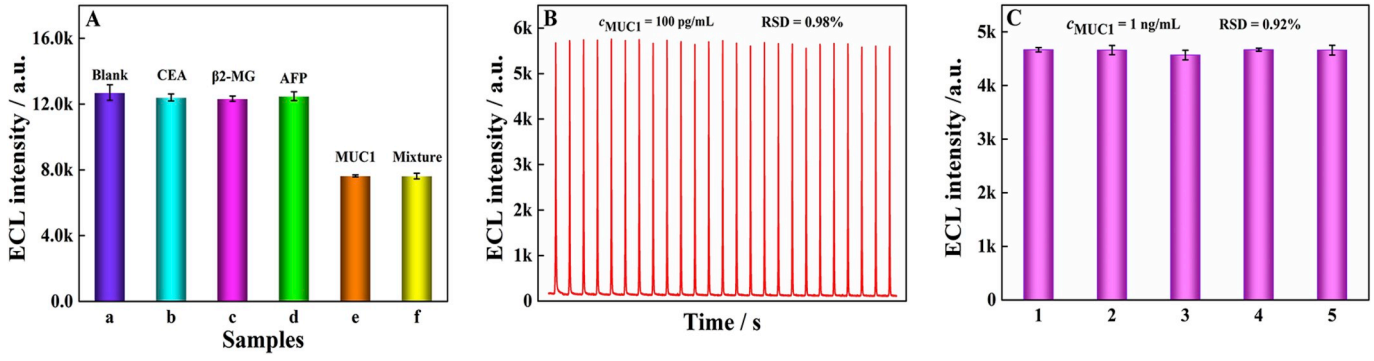

Fig. 7. (A) The selectivity of the proposed biosensor with various interfering substances: (a) blank sample, (b) 10 pg mL^{-1} CEA, (c) 10 pg mL^{-1} β2-MG, (d) 10 pg mL^{-1} AFP, (e) 1 pg mL^{-1} MUC1, (f) the mixture (10 pg mL^{-1} CEA, 10 pg mL^{-1} β2-MG, 10 pg mL^{-1} AFP, and 1 pg mL^{-1} target MUC1). (B) The stability of the developed biosensor (c_{MUC1} = 100 pg mL^{-1}). (C) The reproducibility of the developed biosensor in five parallel assays (c_{MUC1} = 1 ng mL^{-1}).

Declaration of competing interest

The authors declare that they have no known competing financial interests or personal relationships that could have appeared to influence the work reported in this paper.

CRediT authorship contribution statement

Li-Ying Yao: Conceptualization, Data curation, Formal analysis, Investigation, Writing - original draft, Writing - review & editing. **Fang Yang:** Data curation, Formal analysis, Investigation. **Gui-Bing Hu:** Data curation, Investigation. **Yang Yang:** Data curation, Investigation. **Wei Huang:** Data curation, Investigation. **Wen-Bin Liang:** Data curation, Writing - review & editing. **Ruo Yuan:** Project administration, Resources, Writing - review & editing. **Dong-Rong Xiao:** Conceptualization, Project administration, Funding acquisition, Resources, Writing - review & editing, Supervision.

Acknowledgements

This work was supported by the NSFC (21571149) and Venture and Innovation Support Program for Chongqing Overseas Returnees (cx2017007, cx2018026).

Appendix A. Supplementary data

Supplementary data to this article can be found online at https://doi.org/10.1016/j.bios.2020.112099.

References

Carrara, S., Aliprandi, A., Hogan, C.F., Cola, L.D., 2017. J. Am. Chem. Soc. 139, 14605–14610.
Chen, A.Y., Zhao, M., Zhuo, Y., Chai, Y.Q., Yuan, R., 2017. Anal. Chem. 89, 9232–9238.
Chen, H.Y., Xiao, D.R., Fan, L.L., He, J.H., Yan, S.W., Zhang, G.J., Sun, D.Z., Ye, Z.L., Yuan, R., Wang, E.B., 2011. CrystEngComm 13, 7098–7107.
Dai, R.H., Peng, F., Ji, P.F., Lu, K.D., Wang, C., Sun, J.L., Lin, W.B., 2017. Inorg. Chem. 56, 8128–8134.
Deng, C.Y., Pi, X.M., Qian, P., Chen, X.Q., Wu, W.M., Xiang, J., 2017. Anal. Chem. 89, 966–973.
Dick, J.E., Renault, C., Kim, B.-K., Bard, A.J., 2014. J. Am. Chem. Soc. 136, 13546–13549.
Dixit, C.K., Vashist, S.K., O'Neill, F.T., O'Reilly, B., MacCraith, B.D., O'Kennedy, R., 2010. Anal. Chem. 82, 7049–7052.
Han, Z.G., Yang, Z.F., Sun, H.S., Xu, Y.L., Ma, X.F., Shan, D.L., Chen, J., Huo, S.H., Zhang, Z., Du, P.Y., Lu, X.Q., 2019. Angew. Chem. Int. Ed. 58, 5915–5919.
He, J.H., Chen, H.Y., Xiao, D.R., Sun, D.Z., Zhang, G.J., Yan, S.W., Xin, G.H., Yuan, R., Wang, E.B., 2011. CrystEngComm 13, 4841–4845.
He, J.H., Zhang, G.J., Xiao, D.R., Chen, H.Y., Yan, S.W., Wang, X., Yang, J., Wang, E.B., 2012. CrystEngComm 14, 3609–3614.
Hong, Y.N., Lam, J.W.Y., Tang, B.Z., 2011. Chem. Soc. Rev. 40, 5361–5388.
Hu, G.B., Xiong, C.Y., Liang, W.B., Yang, Y., Yao, L.Y., Huang, W., Luo, W., Yuan, R., Xiao, D.R., 2019. Biosens. Bioelectron. 135, 95–101.
Hu, G.B., Xiong, C.Y., Liang, W.B., Zeng, X.S., Xu, H.L., Yang, Y., Yao, L.Y., Yuan, R., Xiao, D.R., 2018. ACS Appl. Mater. Interfaces 10 (18), 15913–15919.
Huang, Y.J., Wang, Z.R., Chen, Z., Zhang, Q.C., 2019. Angew. Chem. Int. Ed. 58, 9696–9711.
Iida, A., Yamaguchi, S., 2009. Chem. Commun. 3002–3004.
Ito, H., Segawa, Y., Murakami, K., Itami, K., 2019. J. Am. Chem. Soc. 141, 3–10.
Jiang, J.J., Lu, Z.Y., Zhang, M.M., Duan, J.G., Zhang, W.W., Pan, Y., Bai, J.F., 2018. J. Am. Chem. Soc. 140, 17825–17829.
Jiang, X.Y., Wang, Z.L., Wang, H.J., Zhuo, Y., Yuan, R., Chai, Y.Q., 2017b. Chem. Commun. 53, 9705–9708.
Jiang, X.Y., Wang, H.J., Zhuo, Y., Yuan, R., Chai, Y.Q., 2017a. Anal. Chem. 89, 4280–4286.
Ko, S.H., Lee, T., Park, H., Ahn, D., Kim, K., Kwon, Y., Cho, S.J., Ryoo, R., 2018. J. Am. Chem. Soc. 140, 7101–7107.
Kufe, D.W., 2009. Nat. Rev. Canc. 9, 874–885.
Li, X., Li, Z.H., Lu, L., Huang, L.M., Xiang, L., Shen, J., Liu, S.Y., Xiao, D.R., 2017. Chem. Eur. J. 23, 10638–10643.
Liu, J.L., Tang, Z.L., Zhang, J.Q., Chai, Y.Q., Zhuo, Y., Yuan, R., 2018. Anal. Chem. 90, 5298–5305.
Liu, J.L., Tang, Z.L., Zhuo, Y., Chai, Y.Q., Yuan, R., 2017. Anal. Chem. 89, 9108–9115.
Liu, J.L., Zhang, J.Q., Tang, Z.L., Zhuo, Y., Chai, Y.Q., Yuan, R., 2019. Chem. Sci. 10, 4497–4501.
Liu, Y., Hou, W.J., Xia, L., Cui, C., Wan, S., Jiang, Y., Yang, Y., Wu, Q., Qiu, L.P., Tan, W. H., 2018. Chem. Sci. 9, 7505.
Luo, J., Xie, Z., Lam, J.W.Y., Cheng, L., Chen, H., Qiu, C., Kwok, H.S., Zhan, X., Liu, Y., Zhu, D., Tang, B.Z., 2001. Chem. Commun. 1740–1741.
Omer, K.M., Bard, A.J., 2009. J. Phys. Chem. C 113, 11575–11578.
Rashidnadimi, S., Hung, T.H., Wong, K.T., Bard, A.J., 2008. J. Am. Chem. Soc. 130 (2), 634–639.
Swanick, K.N., Sandroni, M., Ding, Z., Colman, E.Z., 2015. Chem. Eur. J. 21, 7435–7440.
Tang, B.Z., Zhan, X., Yu, G., Lee, P.P.S., Liu, Y., Zhu, D., 2001. J. Mater. Chem. 11, 2974–2978.
Tomov, T.E., Tsukanov, R., Glick, Y., Berger, Y., Liber, M., Avrahami, D., Gerber, D., Nir, E., 2017. ACS Nano 11, 4002–4008.
Wang, F., Lin, J., Zhao, T.B., Hu, D.D., Wu, T., Liu, Y., 2016. J. Am. Chem. Soc. 138, 7718–7724.
Wang, S.Z., McGuirk, C.M., Ross, M.B., Wang, S.Y., Chen, P.C., Xing, H., Liu, Y., Mirkin, C.A., 2017. J. Am. Chem. Soc. 139, 9827–9830.
Xiao, D.R., Chen, H.Y., Sun, D.Z., He, J.H., Yan, S.W., Yang, J., Wang, X., Yuan, R., Wang, E.B., 2012. CrystEngComm 14, 2849–2858.
Xiong, C.Y., Liang, W.B., Zheng, Y.N., Zhuo, Y., Chai, Y.Q., Yuan, R., 2017. Anal. Chem. 89 (5), 3222–3227.
Yang, W.T., Shen, Y., Zhang, D.Y., Xu, W.J., 2018. Chem. Commun. 54, 10195–10198.
Zeng, W.J., Liao, N., Lei, Y.M., Zhao, J., Chai, Y.Q., Yuan, R., Zhuo, Y., 2018. Biosens. Bioelectron. 100, 490–496.
Zhuo, Y., Liao, N., Chai, Y.Q., Gui, G.F., Zhao, M., Han, J., Xiang, Y., Yuan, R., 2014. Anal. Chem. 86, 1053–1060.